The Journal of Experimental Biology 214, 1692-1698

doi:10.1242/jeb.049148

RESEARCH ARTICLE

The contractile sponge epithelium *sensu lato* – body contraction of the demosponge *Tethya wilhelma* is mediated by the pinacoderm

Michael Nickel[1,*], Corina Scheer[1], Jörg U. Hammel[1], Julia Herzen[2,3] and Felix Beckmann[2]

[1]Institut für Spezielle Zoologie und Evolutionsbiologie mit Phyletischem Museum, Friedrich-Schiller-Universität Jena, Erbertstrasse 1, 07743 Jena, Germany, [2]Helmholtz-Zentrum Geesthacht, Institute of Materials Research, Max-Planck-Strasse 1, 21502 Geesthacht, Germany and [3]Physik-Department, Technische Universität München, James-Franck-Strasse 1, 85748 Garching, Germany

*Author for correspondence (m.nickel@uni-jena.de)

Accepted 19 January 2011

SUMMARY

Sponges constitute one of the two metazoan phyla that are able to contract their bodies despite a complete lack of muscle cells. Two competing hypotheses on the mechanisms behind this have been postulated to date: (1) mesohyl-mediated contraction originating from fusiform smooth muscle-like actinocytes ('myocytes') and (2) epidermal contraction originating in pinacocytes. No direct support exists for either hypothesis. The question of agonist–antagonist interaction in sponge contraction seems to have been completely neglected so far. In the present study we addressed this by studying sponge contraction kinetics. We also tested both hypotheses by carrying out volumetric studies of 3D synchrotron radiation-based x-ray microtomography data obtained from contracted and expanded specimens of *Tethya wilhelma*. Our results support the pinacoderm contraction hypothesis. Should mesohyl contraction be present, it is likely to be part of the antagonist system. We conclude that epithelial contraction plays a major role in sponges. Contractile epithelia *sensu lato* may be regarded as part of the ground pattern of the Metazoa.

Supplementary material available online at http://jeb.biologists.org/cgi/content/full/214/10/1692/DC1

Key words: sponges, agonist, antagonist, contraction, myocyte, pinacoderm.

INTRODUCTION

Among the Metazoa, only the basal Porifera and Placozoa lack muscle cells (Jones, 1962; Nickel, 2010). Cnidarians, in contrast, possess myoepithelia but also striated muscle cells, at least for some members of the Hydrozoa and Scyphozoa (Seipel and Schmid, 2005; Schmidt-Rhaesa, 2007). Myoepithelia are widely regarded as the evolutionary origin of bilaterian muscle cells (Mackie, 1970; Rieger, 1986; Rieger and Ladurner, 2003). However, the evolution of myoepithelia in the first place has hardly been addressed. We currently lack concepts to explain the transition from epithelial cells to specialized contractile epithelia, as demonstrated by a statement by Peter Ax (Ax, 1995): "And finally, an efficient locomotory apparatus emerged by the most simple possible way. Muscle fibres of actin and myosin filaments evolved at the base of normal ectodermal and endodermal cells, thus becoming epithelio-muscle cells by expanding their functionality" [translated by M.N.]. In contrast, scenarios for the evolution of muscle cells from myoepithelia were postulated on the basis of developmental transitions from myoepithelia to subperitoneal fibre muscle cells in echinoderms and annelids, with myoepithelia representing the plesiomorphic condition in the Bilateria (Rieger, 1986; Bartholomaeus, 1994; Rieger and Ladurner, 2003). These findings give rise to questions on the cellular contractility in the ground pattern of the Metazoa. As myoepithelia also represent the plesiomorphic condition in Cnidaria, it seems likely that epithelial contraction – though in a less specialized manner – evolved early in the Metazoa, before the split of all recent metazoan groups. To answer some of these questions on the early evolution of contractility in the Metazoa, comparative morphological and genomic studies in the Porifera and the Placozoa will be essential.

It has been known since ancient times that sponges contract (Aristotélēs, 1498; Lieberkühn, 1859; Schmidt, 1866; Marshall, 1885; Arndt, 1941; Weissenfels, 1990) [for an overview see Nickel (Nickel, 2004; Nickel, 2010)]. Two competing hypotheses have been postulated to explain non-muscular contraction in the Porifera: (1) mesohyl-mediated contraction by spindle-shaped, smooth muscle-like actinocytes, frequently called 'myocytes' (Schmidt, 1866; Pavans de Ceccatty, 1960; Bagby, 1966) [for terminology see Boury-Esnault and Rützler (Boury-Esnault and Rützler, 1997)]; (2) epidermal contraction by pinacocytes (Minchin, 1900; Parker, 1910; Bagby, 1970; Matsuno et al., 1988). Both scenarios are mostly based on indirect evidence, e.g. the smooth muscle-like shape of 'myocytes' (Schmidt, 1866; Pavans de Ceccatty, 1960) and the presence of filaments in both cell types (Bagby, 1966; Bagby, 1970; Pavans de Ceccatty, 1986; Matsuno et al., 1988). The 'myocyte' hypothesis is clearly analogy based, but seems to be the more widely accepted of the two (e.g. Mackie, 1970; Simpson, 1984). The pinacocyte hypothesis is often neglected, despite the fact that Minchin provided an excellent microscopic comparison between contracted and expanded pinacocytes in the calcareous sponge *Clathrina coriacea* (Minchin, 1900).

The question arises as to whether contractility in the Porifera is mechanistically as simple as suggested by these hypotheses. It might well be that both cell types exhibit some contractility, which in both cases remains to be demonstrated on the cellular level. One important mechanistic problem that has never been considered for

sponges is that contractile systems act as agonists and require antagonists in order to reverse contraction. In fact, it is very likely that complex interactions between more than one agonist–antagonist system take place. In this case, sponge contraction kinetics should display typical dynamic patterns with phases of specific kinetic characters.

The aim of our study was to test the two competing hypotheses on sponge contractility. We used synchrotron radiation-based x-ray microtomography (SR-μCT) to perform comparative volumetric studies on contracted and expanded sponges. By addressing total sponge volume, mesohyl volume, canal system volume and skeletal volume, we tested the mesohyl contraction hypothesis. By analysing the total surfaces and calculating surface-to-volume ratios, we tested the pinacoderm contraction hypothesis. Both hypotheses were reviewed visually using 3D-renderings of the SR-μCT datasets. In addition, we aimed to analyse contraction–expansion cycle kinetics in *Tethya wilhelma* in order to test for dynamic patterns of this kind.

The term 'epithelium *sensu lato*': semantic considerations

Contraction of the body or parts thereof requires firm intercellular connections, a quality usually attributed to epithelia. However, at present, it is problematic to use the term epithelium in the context of the Porifera because of semantic ambiguities. The term dates back to the beginning of comparative histology (i.e. Hertwig and Hertwig, 1882; Schneider, 1902) and was initially applied in its widest, functional sense to all animals, including the Porifera for more than a century. Following Rieger (Rieger, 1986) and Starck and Siewing (Starck and Siewing, 1980), the short definition for the epithelium *sensu lato* would be: a polar tissue, with close lateral contacts between cells. Ultrastructural research allowed for the definition to be altered in order to meet homology assumptions. Following Rieger (Rieger, 1986), Ax and colleagues (Ax et al., 1989; Ax, 1995) and Tyler (Tyler, 2003), such an extended short definition *sensu stricto* would be: a polar tissue underlined by basal membrane, with close lateral contacts between cells mediated by belt desmosomes. This fairly recent re-definition resulted in the occupation of the established terminus by new attributes and makes sense only in the context of phylogenetic systematics. Semantically, however, such re-definitions of existing terms generally create difficulties, such as in the functional usage of the term epithelium regarding the Porifera. To date, most members of the Porifera lack a basal membrane and the presence of belt-like junctions is controversial (Tyler, 2003; Leys et al., 2009; Ereskovsky et al., 2010); therefore, their characters were addressed as non-epithelial, epitheloid or non-tissue grade of organization, which is semantically imprecise. This specific semantic problem is part of the 'linguistic problem of morphology', which is currently being widely discussed (i.e. Vogt et al., 2010). However, as the sponge pinacoderm displays the most important features to fulfill the functions of delimiting the inner body compartment, including the generation of an electrical transepithelial resistance (Adams et al., 2010), it fully meets the definition for a functional epithelium *sensu lato* provided above. In addition, it is ontogenetically derived from the sponge blastula epithelium (Leys et al., 2009; Ereskovsky et al., 2010). Consequently, the term epithelium should be used *sensu lato* as it has been for more than 100 years (Schmidt, 1866; Schneider, 1902; Starck and Siewing, 1980).

MATERIALS AND METHODS

Sponge specimens

All investigations were carried out upon specimens of *Tethya wilhelma*; Sarà, Sarà, Nickel and Brümmer 2001 (Demospongiae, Hadromerida, Tethyidae). Sponges originated from their type locality, the aquarium of the Zoological-Botanical Garden Wilhelma Stuttgart (Germany). Because it reproduces asexually by budding, *T. wilhelma* was permanently cultured in the laboratory in Jena in tropical seawater aquaria under constant moderate flow conditions at a temperature of 24°C and a light regime of 12 h day and night. Artificial seawater (Tropic Marine, Wartenberg, Germany; dissolved in demineralized water) was partially renewed every few weeks. During cultivation, sponges were fed on a daily basis using finely dispersed commercial aquarium invertebrate food ('Artificial Plankton' Aquakultur Genzel, Freiberg am Neckar, Germany).

Analysis of contraction cycle kinetics

Kinetic data from a previously published extended dataset of digital time lapse images covering 13 contraction–expansion cycles of *T. wilhelma* (Nickel, 2004) were normalized and reanalysed using Microsoft Excel. Each cycle was normalized to the maximum (A_{max}=1) and minimum (A_{min}=0) projected body area of the sponge. A mean contraction cycle and standard deviation were calculated, resulting in relative expansion E over relative contraction time with t_0=E_{min}. The change over time of relative expansion ΔE was calculated and resulted in the relative velocity v of contraction and expansion (v=ΔE=dE/dt). The change over time of relative velocity v was calculated and resulted in the relative acceleration of contraction and expansion (a=$\Delta\Delta E$=Δv=dv/dt). The values of E, v and a were plotted against relative contraction time to correlate conspicuous changes in these graphs and allow conclusions to be drawn on kinetic changes during the contraction and expansion phases of the cycles.

Morphological analysis

One fully expanded and one completely contracted sponge specimen of *T. wilhelma* were processed for synchrotron radiation-based x-ray microtomography (Nickel et al., 2006; Hammel et al., 2009). Contraction was induced by glutamate application (Ellwanger et al., 2007). Specimens were immediately shock frozen in liquid nitrogen and subsequently fixed by freeze-substitution in a Leica AFS (Leica, Bensheim, Germany) in methanol with 1% OsO_4, 2.5% glutaraldehyde and 2.5% distilled water (modified from Müller et al., 1980) at –80°C for 68.5 h; they were then warmed to 0°C at a constant rate of 40°C h^{-1}. The samples were washed twice in methanol and three times in dimethoxyphenol (DMP). The samples were transferred to approximately 25 ml DMP in a dish, which was partly covered by a glass slide, and allowed to dry slowly inside an extraction hood overnight. Dried samples were imaged as described previously (Nickel et al., 2006) by synchrotron radiation-based x-ray microtomography operated by HZG (Beckmann et al., 2008) at beamline BW2 of the storage ring DORIS III at Deutsches Elektronen Synchrotron (DESY, Hamburg, Germany) at 14.5 keV, followed by tomographic reconstruction, which resulted in 32-bit floating point image stacks with a voxel size of 3.75 μm^3, representing a measured resolution of 5.7 μm^3 per voxel. For virtual reconstruction and volume rendering we used VG studio MAX 2.0 (Volume Graphics, Heidelberg, Germany). Volumetric and surface analysis was performed using a custom-made macro routine in ImageJ, based on x-ray absorption values, which were coded as 8-bit greyscale image stacks after conversion from the original 32-bit floating point image data, following a previously published routine (Nickel et al., 2006; Hammel et al., 2009). For a better comparison, the volumes of the canal system, mesohyl and skeleton are provided as percentile values relative to the total sponge volume. As it was not possible to choose two specimens with identical expanded

volumes, we normalized our data to the skeleton volumes for direct comparison. In this approach, we assumed a relatively stable proportion between skeleton and mesohyl. Indirect evidence has been provided for such a correlation between extracellular matrix synthesis and spicule production (Krasko et al., 2000). Therefore, normalizing the volume data against the skeleton illustrates the comparable relative amount of volume change of the mesohyl and the canal system. In addition, the directly comparable ratio between pinacoderm surface area and mesohyl volume as well as total sponge volume was calculated.

After microtomographic imaging the samples were re-used for scanning electron microscopy (SEM) histology (Weissenfels, 1982; Hammel et al., 2009). In brief, samples were transferred to 100% ethanol, embedded into styrene-methacrylate and semi-thin sectioned until a median position was reached. The last sections of the series were stained by Toluidine Blue and imaged on a Zeiss Axiolab equipped with a Pixellink BF623 firewire camera. The remaining embedded sponge fragment was xylene treated to dissolve the plastic, transferred to 100% ethanol and critical point dried. SEM images were taken on a Philips XL30ESEM.

RESULTS

Contraction cycle analysis

Graphs of 13 consecutive contraction cycles were normalized to their projected body area, resulting in plots of the relative expansion E over time. E=1 represents the maximum body expansion at the beginning and the end of each cycle. E=0 represents the maximum body contraction of each cycle, which was concurrently defined as relative contraction cycle time t_0=0 s (Fig. 1A, central arrow). The overlay of these normalized kinetics graphs and the movies of 13 consecutive contraction cycles of *T. wilhelma* reveal their kinetic uniformity (Fig. 1A; supplementary material Movie 1). The kinetic uniformity is most obvious around E_{min}, between t=–1000 s and t=1000 s. In contrast, all 13 cycle graphs display conspicuous slope changes (‘shoulders’) during contraction at around t=–1000 s (Fig. 1A, left arrow) and during expansion at around t=1000 s (Fig. 1A, right arrow).

In order to analyse the stability of these ‘shoulder’ characteristics within the data, we plotted a mean contraction cycle graph, which clearly retained the shoulder characteristics at t=–1000 s and t=1000 s (Fig. 1B, top graph). In addition, we calculated the first and second time derivatives in order to visualize the relative velocity of contraction and expansion v (first time derivative; v=dE/dt) and the relative acceleration of contraction and expansion a (second time derivative; a=dv/dt). Both ‘shoulders’ of E are represented in the first time derivative as prominent changes of relative velocity v at t=–1000 s and t=1000 s (Fig. 1B, middle graph). Maximum acceleration a_{max} of contraction occurs around t=–800 s (Fig. 1B, bottom graph). Immediately after the sponge reaches E_{min}, expansion starts with maximum acceleration a_{max} of expansion (Fig. 1B, bottom graph).

Based on these characteristics of the dynamics of relative expansion E and relative velocity v, the cycle can be subdivided into four kinetic sub-phases (SP) which differ mainly in their mean and maximum relative velocities $|v|$. Sub-phases SP1 and SP4 display equal relative $|v|$ with $0<|v|<0.5$, which is significantly lower than $|v|$ of SP2 and SP3 where $0<|v|<1.5$ and $0<|v|<1$, respectively. Although the relative velocities $|v|$ of SP2 and SP3 are similar, contraction in SP2 is slightly faster than expansion in SP3.

Anatomy of contraction

The comparison between expanded and contracted *T. wilhelma* anatomy revealed conspicuous changes (semi-thin sections as

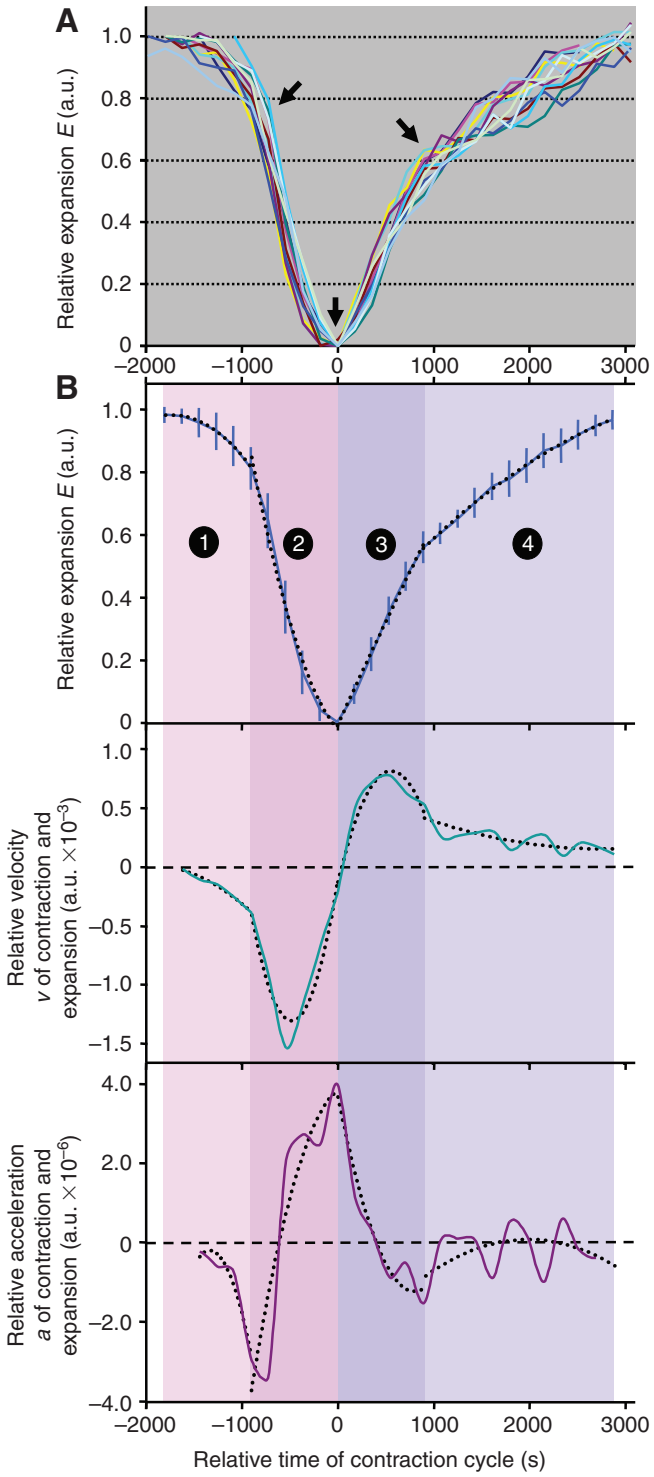

Fig. 1. Contraction kinetics of *Tethya wilhelma* over time. (A) Relative expansion E; stacked graphs of 13 consecutive cycles (see supplementary material Movie 1). Central arrow at t=0 indicates the reference point of the minima of all stacked graphs. Right and left arrows: conspicuous slope changes (‘shoulders’) during contraction and expansion. (B) Relative expansion E (top); data are means and s.d. calculated from the graphs presented in A; sub-phases (SP) 1–4 are colour coded. Relative velocity v (middle) and relative acceleration a (bottom) of contraction and expansion. Characteristics of sub-phases: mean velocities similar in SP1 and SP4: v_1=–0.2×10^{-3} (R^2=0.8916), v_4=0.2×10^{-3} (R^2=0.9856); higher velocities in SP2 and SP3: v_2=–1×10^{-3} (R^2=0.953), v_3=0.6×10^{-3} (R^2=0.9961). a.u., arbitrary units.

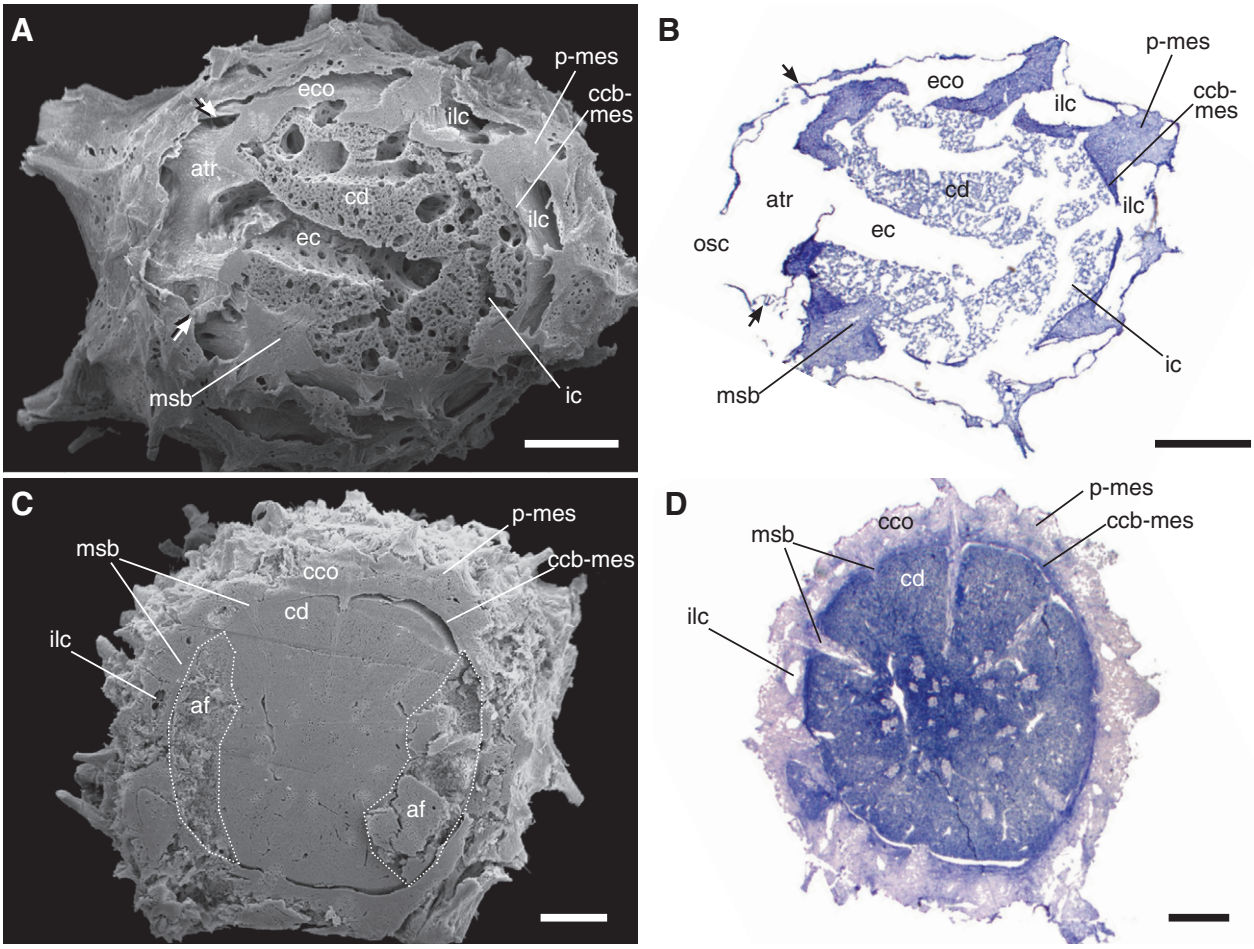

Fig. 2. Comparison between contracted (A,B) and expanded (C,D) specimens of *T. wilhelma* using SEM imaging of section planes (A,C) and light microscopy of the corresponding stained semi-thin sections (B,D). The canal system is clearly structured in the expanded specimen, while in the contracted specimen, canal structures are only partially distinguishable. Note the difference in density (A *vs* C) and staining intensity (B *vs* D) of the peripheral mesohyl (p-mes) in the cortex of expanded and contracted specimens. Abbreviations: af, artefact on section surface (mechanical damage after critical point drying); atr, atrium; ccb-mes, mesohyl of the cortex–choanoderm boundary; cco, contracted cortex; cd, choanoderm; ec, excurrent canal; eco, expanded cortex; ic, incurrent canal; ilc, incurrent lacunae; mes, mesohyl; msb, megasclere bundle; osc, oscule; p-mes, peripheral mesohyl. Arrows: barriers between incurrent and excurrent lacunae. Scale bars: 250 μm. Images B and D were enhanced in contrast in order to distinguish canal structures from the mesohyl as clearly as possible.

viewed by light microscopy and corresponding section planes as viewed by SEM in Fig. 2; virtual 3D reconstruction based on SR-μCT data in Fig. 3). These changes mainly concern the canal system (Fig. 2 and Fig. 3A,C).

In the expanded state, all canal system elements are inflated (Fig. 2A,B and Fig. 3A). The cortex is dominated by inhalant lacunae (Fig. 2A,B; ilc) which are underlined by strongly stained collagen layers of the mesohyl at the cortex–choanoderm boundary (Fig. 2A,B; ccb-mes). The peripheral mesohyl of the expanded sponge stains only slightly weaker (Fig. 2A,B; p-mes). Exhalant lacunae are solely present around the oscule. Both lacunae types are functionally separated by pinacoderm–mesohyl barriers (arrows in Fig. 2A,B). The cortical mesohyl is mainly restricted to thin sheets between the exopinacoderm and the lacunar endopinacoderm, and a collagen-rich sphere at the cortex–choanoderm boundary. The cortical mesohyl around the main skeleton (megasclere bundles) is solid and collagen rich, resulting in prominent Toluidine Blue staining. The choanosome is dominated by finer inhalant and exhalant canals connected to numerous choanocyte chambers, creating a porous visual impression (Fig. 2A,B and Fig. 3A).

In the contracted state, the cortex and choanoderm both appear to be solid, with only a few lacunae and canals visible (Fig. 2C,D and Fig. 3C). The volume of the canal system is minimized, with the smaller canals almost completely collapsed and hardly visible. The atrium, the largest exhalant canals and some cortical incurrent lacunae remain identifiable despite their reduced volumes (see atr and ec in Fig. 3C). In contrast to the expanded sponge, the contracted cortex displays only the small remains of incurrent lacunae, but is generally characterized by a less dense, weaker stained collagen meshwork of the peripheral mesohyl (Fig. 2C,D; p-mes), which is distinguishable from the denser and strongly stained collagen of the mesohyl at the cortex–choanoderm boundary (Fig. 2C,D; ccb-mes).

Morphometrics of contraction

Our anatomical observations are supported by volumetric measurements using the same SR-μCT datasets of the expanded and contracted specimens.

The expanded sponge (Fig. 3B and Fig. 4A) is dominated by the canal system (~72%), significantly exceeding mesohyl (~28%) and skeleton (~3%) volumes. In contrast, the contracted sponge (Fig. 3D

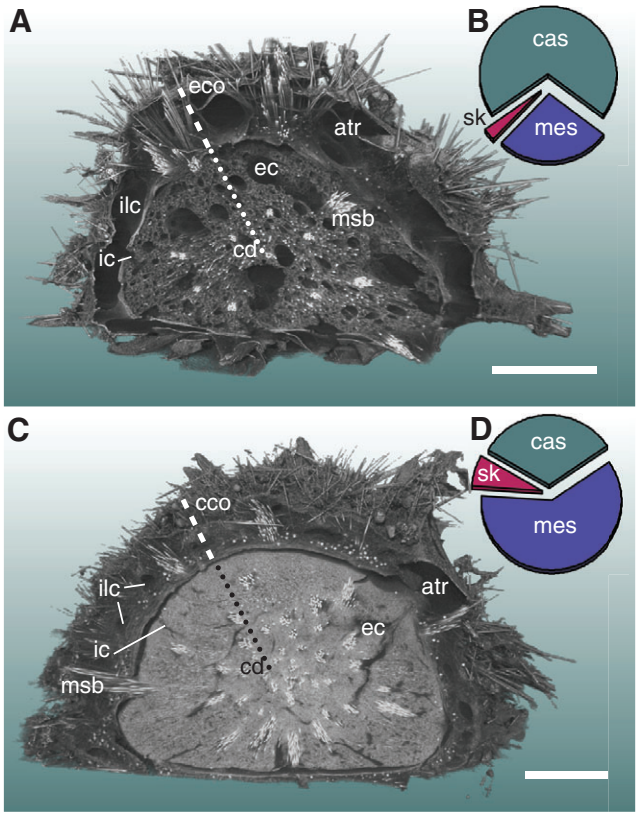

Fig. 3. Comparison between contracted (A,B) and expanded (C,D) specimens of *T. wilhelma* using virtual reconstruction of synchrotron radiation-based x-ray microtomography (SR-μCT) datasets (A,C). Volumetric measurements of anatomical structures are presented as pie diagrams (B,D; direct comparison shown in Fig. 4A). Abbreviations: atr, atrium; cas, canal system; cco, contracted cortex; cd, choanoderm; ec, excurrent canal; eco, expanded cortex; ic, incurrent canal; ilc, incurrent lacunae; mes, mesohyl; msb, megascler bundle; sk, skeleton. Dashed/dotted lines: barriers between incurrent and excurrent lacunae. Scale bars: 500 μm.

and Fig. 4A) is dominated by the mesohyl (~60%), which is almost double the canal system volume (~32%). The skeleton occupies ~7%.

We standardized both datasets by normalizing them to the skeleton (Fig. 4B), which is the only body structure not affected by contraction. The mesohyl-to-skeleton volume ratio remains almost constant at between ~8:1 and ~9:1 regardless of the state of contraction. In contrast, the canal system-to-skeleton volume ratio decreases from ~23:1 in the expanded state to ~4:1 in the contracted state.

Surface-to-volume-ratios

Surface-to-volume ratios (Fig. 4C) allow a direct comparison between the expanded and contracted sponges. From the SR-μCT data, we measured the surface areas. By relating these to the total volume, we calculated that the pinacoderm-to-total sponge volume ratio changes from ~127:1 in the expanded sponge to ~100:1 in the contracted sponge. In order to exclude the impact of the highly variable canal system, we calculated the pinacoderm-to-mesohyl ratio, which at ~458:1 in the expanded sponge and ~166:1 in the contracted sponge undergoes a significant 2.75 times decrease during contraction.

DISCUSSION

Contraction kinetics

Our kinetic data show that contraction and expansion can each be subdivided into two sub-phases (SP). The differences in contraction and expansion velocities in sub-phases SP1 and SP2 compared with those in sub-phases SP3 and SP4 imply that the situation is complex with regard to the cellular agonists and antagonists of contraction and expansion. From our morphometric data we conclude that contraction in SP1 and SP2 is generated by the sponge surfaces, i.e. the pinacocytes. The lower contraction velocity of SP1 suggests a systemic resistance to contraction that is probably generated by the water in the canals and lacunae. The pressure differential caused by the choanocytes may also play a role. Eventually, during or towards the end of SP1 the choanocytes stop pumping, thus decreasing the systemic pressure and permitting the more rapid contraction observed in SP2.

The high expansion velocity in SP3 suggests a specific fast-acting antagonist system that works to produce expansion forces. Functional and structural considerations point towards the mesohyl as the antagonist. Expansive forces may be produced by contractile cells such as the actinocytes and/or by visco-elastic energy stored within the collagenous matrix during contraction (Vogel, 2003). The slower expansion of SP4 also suggests a morphological systemic resistance. The lower expansion velocity may demonstrate antagonist force limits and/or reveal the contribution of the pressure increase caused by the onset of choanocyte pumping activity. The increasing water pressure in the narrow canals might inflate the sponge towards the end of the cycle.

In conclusion, kinetic data from *T. wilhelma* support a bi-phasic model of contraction and expansion with (1) a cellular/tissue-based antagonistic contractile apparatus that mediates the main contraction

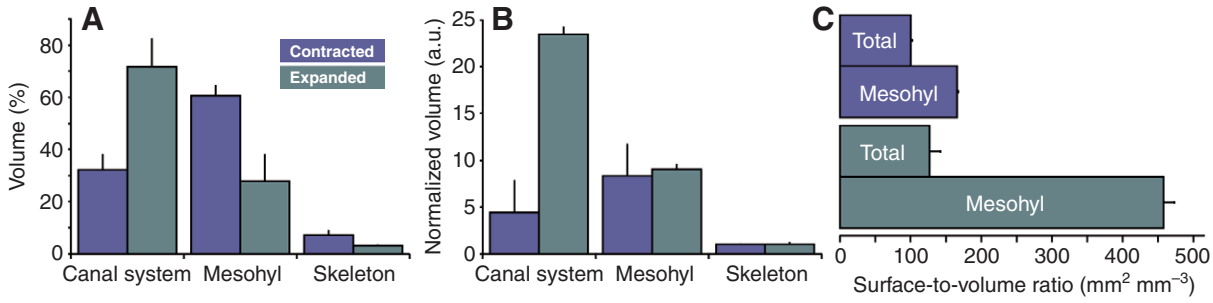

Fig. 4. Direct comparison of volumetric measurements of anatomical structures between contracted and expanded sponges (A) and after normalization to the skeletal volume (B). Surface-to-volume ratios are presented for the pinacoderm in relation to total sponge volume and mesohyl volume in both states (C). a.u., arbitrary units.

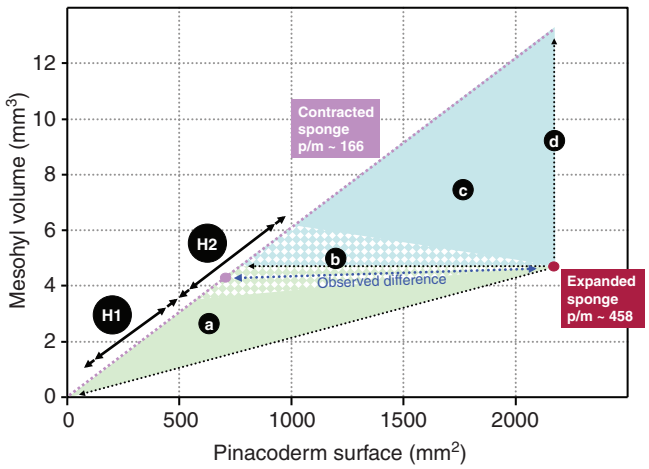

Fig. 5. Relationship between pinacoderm surface area and mesohyl volume. The expanded specimen with a pinacoderm-to-surface ratio (p/m) of ~458 (dark red dot) is compared with the theoretical possible combinations of mesohyl volume and pinacoderm surface, which result in a p/m of ~166 (mauve dotted line). The green area (a) defines a theoretical morphospace of contraction that is characterized by a combined decrease of pinacoderm area and mesohyl volume. The blue area (c) represents the theoretical contraction morphospace in cases of pinacoderm area decrease combined with mesohyl volume increase. Two distinct cases are marked by dotted arrows: constant mesohyl volume combined with decreasing pinacoderm area (b); constant pinacoderm area with increasing mesohyl volume (d), which represents a theoretical case of no biological significance. The expected approximate ranges for the dominance of mesohyl contraction (H1) and pinacoderm contraction (H2) are indicated by double-headed arrows. Additionally, the area of the approximate morphospace for pinacoderm contraction is filled by white diamonds. The measured values of the contracted sponge were scaled according to those of the expanded sponge and plotted as a mauve dot. The observed difference (blue dotted arrow) between the contracted and expanded sponge is close to case b (constant mesohyl combined with contractile pinacoderm) and lies within the morphospace of H2 (domination by pinacoderm contraction).

and expansion, and (2) the water pressure generated by the choanocyte chambers. The latter seems (a) to generate resistance against contraction during the initial contraction phase, and (b) to add additional water pressure, which might expand the canals to their fully extended state.

Evidence for the dominance of pinacoderm contraction

The microtomography imaging followed by 3D virtual reconstruction and morphometrics carried out in the present study demonstrate that the major changes during contraction affect the sponge canal system volume, not the mesohyl. The hypothesis of mesohyl contraction (Schmidt, 1866; Pavans de Ceccatty, 1960; Bagby, 1966) is not supported quantitatively by our data on the basis of our absolute and normalized volumetric data. In contrast, the hypothesis of pinacoderm contraction (Minchin, 1900; Parker, 1910; Bagby, 1970; Matsuno et al., 1988) is strongly supported by our volume and surface analysis, in particular by the pinacocyte surface-to-mesohyl volume ratios, which can be directly compared among specimens, in combination with the evidence for a constant mesohyl volume. The same volume of mesohyl is surrounded by 2.75 times more pinacocyte surface in the expanded state than in the contracted state. This difference in pinacoderm-to-mesohyl ratio of ~458:1 in the expanded sponge and ~166:1 in the contracted sponge can be explored with a graphical morphospace diagram, which plots the mesohyl volume against the pinacoderm surface (Fig. 5) and represents all theoretically possible geometric cases. Consequently, such a morphospace diagram contains all biologically significant combinations of mesohyl volume and pinacoderm area, as well as additional combinations that are theoretically possible but biologically nonsensical. One nonsensical example would be the assumption of a constant pinacoderm that does not change area at all (whether actively or passively) in combination with an increasing mesohyl volume (see Fig. 5, d). One ideal case is of biological significance: the combination of constant mesohyl volume and decreasing pinacoderm area (see Fig. 5, b). The observed difference between the contracted and expanded sponges comes close to this ideal case and lies within the theoretically expected morphospace for pinacoderm contraction.

Such surface reductions without significant volume changes (isovolumetric) can be explained by geometric shape changes. A simple example would be the isovolumetric transformation of a cube into a sphere. Because a cube displays a larger surface area to volume ratio than a sphere, such an isovolumetric transformation requires a decreasing surface area (i.e. a contractile surface). However, as demonstrated by our 3D renderings, SEM images and histological sections (Figs 2 and 3), the geometric changes that affect the canal system of *T. wilhelma* during contraction are more complex than in this example. In the future, detailed finite element modelling based on 3D data of contracted and expanded sponge tissue might lead to a better understanding of this issue, as has been the case for muscle contraction (Oomens et al., 2003).

Which physiological effects might be connected to pinacoderm-mediated sponge contractility? Although we cannot provide direct evidence to date, it seems likely that during contraction of *T. wilhelma*, water pumping completely stops. Based on the strong morphological changes during contraction, we can assume strong physiological effects of the surface area reduction in relation to the mesohyl, which would probably be connected to physiological changes occurring during pumping arrest. It has been shown before that temporal anoxic phases within the sponges occur and might be related to metabolism of symbiotic microorganisms (Hoffmann et al., 2005). Taken together, gas exchange, food particle uptake and excretion are expected to be temporally reduced to a minimum during contraction. In this context, it is interesting to compare the contraction kinetics (Fig. 1) and note that the strongest contraction is not retained by the sponge, but is simply a transitional state.

CONCLUSION

In conclusion, our data strongly support the pinacoderm contraction hypothesis for the Demospongiae. If spindle-shaped mesohyl cells (presently referred to as actinocytes, formerly known as ‘myocytes’) (see Boury-Esnault and Rützler, 1997) are involved in the process at all, it seems to be more likely that they act as antagonists, mediating sponge expansion.

We tested the two major competing sponge contraction hypotheses quantitatively – for the first time – and found further, indirect but strong support for the contractile pinacoderm in sponges. Our results raise general questions about the evolution of contractility in metazoans. The pinacoderm can be regarded as ‘epitheloid’, or in other words as an epithelium *sensu lato* (Starck and Siewing, 1980; Rieger, 1986; Leys et al., 2009). This gives rise to the question of whether a contractile epithelium *sensu lato* is part of the ground pattern of the Metazoa, and more specifically whether myoepithelia are derived from it (Rieger, 1986). Pinacocytes are large and extremely flat (Simpson, 1984). Thus, their anatomy differs significantly from that of myoepithelial cells of the Cnidaria and other animals. Although they contain highly ordered and presumably

contractile filaments (Bagby, 1970), and may be traversed by extended actin networks (Pavans de Ceccatty, 1986; Elliott and Leys, 2007), their contractility remains to be verified functionally and ultrastructurally. Consequently, our results demonstrate the urgent need to understand the contractile mechanism of pinacocytes on the cellular level. Further studies into the ultrastructure and functional morphology of the pinacocytes in Porifera and the epithelia in Placozoa will help shed light on the evolutionary origin of contractility in the Metazoa.

ACKNOWLEDGEMENTS

We would like to thank Martin S. Fischer, Katja Felbel and Benjamin Weiss (all Freidrich-Schiller-Universität Jena), Michael Schweikert and Kornelia Ellwanger (both Universität Stuttgart) for their input in discussions and technical assistance, and Lucy Cathrow for improving the language. Jasper M. de Goeij and one additional anonymous reviewer provided valuable comments that helped us to improve the manuscript. M.N. received financial support and infrastructure access through DESY grants I-20051083 and I-20060252.

REFERENCES

Adams, E. D. M., Goss, G. G. and Leys, S. P. (2010). Freshwater sponges have functional, sealing epithelia with high transepithelial resistance and negative transepithelial potential. *PLoS ONE* **5**, e15040.

Aristotélēs (1498). De natura animalium libri novem; de partibus animalium libri quatuor; de generatione animalium libri quinqui. In *Domini Octaviani Scoti* (ed. T. Gaza). Elektronic facsimile: Bibliotheque National de France: http://gallica.bnf.fr/ark:/12148/bpt6k58363n.

Arndt, W. (1941). Lebendbeobachtungen an Kiesel und Hornschwämmen des Berliner Aquariums. *Zool. Gart. Leipzig* **13**, 140-166.

Ax, P. (1995). *Das System der Metazoa*. Stuttgart: Gustav Fischer Verlag.

Ax, P., Sopott-Ehlers, B., Ehlers, U. and Bartolomaeus, T. (1989). Was leistet das Elektronenmikroskop für die Aufdeckung der Stammesgeschichte der Tiere? In *Akademie der Wissenschaften und der Literatur Mainz: 1949-1989*, pp. 73-86. Stuttgart: Franz Steiner Verlag.

Bagby, R. M. (1966). The fine structure of myocytes in the sponges *Microciona prolifera* (Ellis and Sollander) and *Tedania ignis* (Duchassaing and Michelotti). *J. Morphol.* **118**, 167-182.

Bagby, R. M. (1970). The fine structure of pinacocytes in the marine sponge *Microciona prolifera*. *Cell Tissue Res.* **105**, 579-594.

Bartholomaeus, T. (1994). On the ultrastructure of the coelomic lining in the Annelida, Sipuncula and Echiura. *Microfauna Mar.* **9**, 171-220.

Beckmann, F., Herzen, J., Haibel, A., Müller, B. and Schreyer, A. (2008). High density resolution in synchrotron-radiation-based attenuation-contrast microtomography. *Proc. SPIE* **7078**, 70781D.

Boury-Esnault, N. and Rützler, K. (1997). Thesaurus of sponge morphology. *Smithson. Contrib. Zool.* **596**, 1-55.

Elliott, G. R. D. and Leys, S. P. (2007). Coordinated contractions effectively expel water from the aquiferous system of a freshwater sponge. *J. Exp. Biol.* **210**, 3736-3748.

Ellwanger, K., Eich, A. and Nickel, M. (2007). GABA and glutamate specifically induce contractions in the sponge *Tethya wilhelma*. *J. Comp. Physiol. A* **193**, 1-11.

Ereskovsky, A., Konyukov, P. and Tokina, D. (2010). Morphogenesis accompanying larval metamorphosis in *Plakina trilopha* (Porifera, Homoscleromorpha). *Zoomorphology* **129**, 21-31.

Hammel, J. U., Herzen, J., Beckmann, F. and Nickel, M. (2009). Sponge budding is a spatiotemporal morphological patterning process: insights from synchrotron radiation-based x-ray microtomography into the asexual reproduction of *Tethya wilhelma*. *Front. Zool.* **6**, 19.

Hertwig, O. and Hertwig, R. (1882). Die Coelomtheorie. Versuch einer Erklärung des mittleren Keimblattes. *Jena. Z. Naturwiss.* **15**, 1-150.

Hoffmann, F., Larsen, O., Thiel, V., Rapp, H. T., Pape, T., Michaelis, W. and Reitner, J. (2005). An anaerobic world in sponges. *Geomicrobiol. J.* **22**, 1-10.

Jones, C. W. (1962). Is there a nervous system in sponges? *Biol. Rev.* **37**, 1-50.

Krasko, A., Lorenz, B., Batel, R., Schroeder, H. C., Mueller, I. M. and Mueller, W. E. G. (2000). Expression of silicatein and collagen genes in the marine sponge Suberites domuncula is controlled by silicate and myotrophin. *Eur. J. Biochem.* **267**, 4878-4887.

Leys, S. P., Nichols, S. A. and Adams, E. D. M. (2009). Epithelia and integration in sponges. *Integr. Comp. Biol.* **49**, 167-177.

Lieberkühn, N. (1859). Neue Beiträge zur Anatomie der Spongien. *Arch. Anat. Physiol.* **30**, 353-358, 515-529.

Mackie, G. O. (1970). Neuroid conduction and the evolution of conducting tissues. *Q. Rev. Biol.* **45**, 319-332.

Marshall, W. (1885). Coelenterata, Porifera, Tetractinellidae; Tafel XLVII. In *Zoologische Wandttafeln der wirbellosen Thiere* (ed. R. Leuckart). Kassel: Verlag von Theodor Fischer.

Matsuno, A., Ishida, H., Kuroda, M. and Masuda, Y. (1988). Ultrastructures of contractile bundles in epithelial cells of the sponge. *Zool. Sci.* **5**, 1212.

Minchin, E. (1900). Sponges. In *A Treatise on Zoology. Part II The Porifera and Coelentera* (ed. E. R. Lancester), pp. 1-178. London: Adam & Charles Black.

Müller, M., Marti, T. and Kriz, S. (1980). Improved structural preservation by freeze-substiution. In *Electron Microscopy*, Vol. 2, Proceedings of the 7th European Congress on Electron Microscopy (ed. P. Brederoo and W. de Priesters), pp. 720-721. Leiden: Elsevier Science.

Nickel, M. (2004). Kinetics and rhythm of body contractions in the sponge *Tethya wilhelma* (Porifera: Demospongiae). *J. Exp. Biol.* **207**, 4515-4524.

Nickel, M. (2010). Evolutionary emergence of synaptic nervous systems: what can we learn from the non-synaptic, nerveless Porifera? *Invertebr. Biol.* **129**, 1-16.

Nickel, M., Donath, T., Schweikert, M. and Beckmann, F. (2006). Functional morphology of *Tethya* species (Porifera): 1. Quantitative 3D-analysis of *Tethya wilhelma* by synchrotron radiation based X-ray microtomography. *Zoomorphology* **125**, 209-223.

Oomens, C. W. J., Maenhout, M., van Oijen, C. H., Drost, M. R. and Baaijens, F. P. (2003). Finite element modelling of contracting skeletal muscle. *Philos. Trans. R. Soc. Lond. B* **358**, 1453-1460.

Parker, G. H. (1910). The reactions of sponges, with a consideration of the origin of the nervous system. *J. Exp. Zool.* **8**, 765-805.

Pavans de Ceccatty, M. (1960). Les structures cellulaires de type nerveux et de type musculaire de l'éponge siliceuse *Tethya lyncurium* Lmck. *C. R. Acad. Sci. Paris* **251**, 1818-1819.

Pavans de Ceccatty, M. (1986). Cytoskeletal organization and tissue patterns of epithelia in the sponge *Ephydatia mülleri*. *J. Morphol.* **189**, 45-66.

Rieger, R. (1986). Über den Ursprung der Bilateria: die Bedeutung der Ultrastrukturforschung für ein neues Verstehen der Metazoenevolution. *Verh. Dtsch. Zool. Ges.* **79**, 31-50.

Rieger, R. M. and Ladurner, P. (2003). The significance of muscle cells for the origin of mesoderm in bilateria. *Integr. Comp. Biol.* **34**, 47-54.

Schmidt, O. (1866). *Zweites Supplement der Spongien des Adriatischen Meeres enthaltend die Vergleichung der Adriatischen und Britischen Spongiengattungen*. Leipzig: Verlag von Wilhelm Engelmann.

Schmidt-Rhaesa, A. (2007). *The Evolution of Organ Systems*. Oxford: Oxford University Press.

Schneider, K. (1902). *Lehrbuch der vergleichenden Histologie der Tier*e. Jena: Verlag G. Fischer.

Seipel, K. and Schmid, V. (2005). Evolution of striated muscle: jellyfish and the origin of triploblasty. *Dev. Biol.* **282**, 14-26.

Simpson, T. L. (1984). *The Cell Biology of Sponges*. New York: Springer Verlag.

Starck, D. and Siewing, R. (1980). Concerning the discussion of the terms mesenchym and mesoderm. *Zool. Jahrb. Abt. Anat. Ontogenie Tiere* **103**, 374-388.

Tyler, S. (2003). Epithelium-the primary building block for metazoan complexity. *Integr. Comp. Biol.* **43**, 55-63.

Vogel, S. (2003). *Comparative Biomechanics. Life's Physical World*. Princeton: Princeton University Press.

Vogt, L., Bartolomaeus, T. and Giribet, G. (2010). The linguistic problem of morphology: structure versus homology and the standardization of morphological data. *Cladistics* **26**, 301-325.

Weissenfels, N. (1982). Scanning electron microscope histology of spongy *Ephydatia fluviatilis* material. *Microsc. Acta* **85**, 345-350.

Weissenfels, N. (1990). Condensation rhythm of fresh-water sponges (Spongillidae, Porifera). *Eur. J. Cell Biol.* **53**, 373-383.